Research Article

Journal of RAMAN SPECTROSCOPY

Received: 12 October 2010 Accepted: 21 February 2011 Published online in Wiley Online Library: 3 May 2011

(wileyonlinelibrary.com) DOI 10.1002/jrs.2949

A theoretical investigation of super-resolution CARS imaging via coherent and incoherent saturation of transitions†

Willem P. Beeker,[a] Chris J. Lee,[a] Klaus J. Boller,[a]* Petra Groß,[b] Carsten Cleff,[b] Carsten Fallnich,[b] Herman L. Offerhaus[c] and Jennifer L. Herek[c]

We review two approaches to achieving sub-diffraction-limited resolution coherent anti-Stokes Raman scattering (CARS) microscopy (Beeker *et al.*, *Opt. Express*, 2009, *17*, 22632 and Beeker *et al.*, *J. Herek, Phys. Rev. A*, 2010, *81*, 012507). We performed a numerical investigation, based on the density matrix model, of the CARS emission process and identified two modified CARS experiments that lead to sub-diffraction-limited resolution images. At the heart of both processes is the spatial manipulation of the coherence between the ground state and the vibrational state being probed by the CARS process via a control state and a control laser that is resonant with the ground state to control state transition. We find two possible regimes of operation: in the first regime, the control and vibrational states are coupled via incoherent processes so that the populations of the two states reach equilibrium very quickly compared to the relevant coherence times. Under these conditions, pre-populating the control state provides a saturable suppression of the coherence between the ground state and the vibrational state, suppressing CARS emission. By using a donut mode to pre-populate the control state, CARS is suppressed everywhere but the central node, allowing sub-diffraction-limited resolution imaging. In the second regime, the control state has a rather long coherence lifetime, and the resonant laser drives Rabi oscillations that periodically deplete the ground state. As a result, the CARS emission process is amplitude-modulated, which appear as sidebands on the CARS spectrum. By a process of *spectral resolution* and trilateration, sub-diffraction-limited resolution images can be obtained. **Copyright © 2011 John Wiley & Sons, Ltd.**

Supporting information may be found in the online version of this article.

Keywords: coherent anti-Stokes Raman Scattering; imaging; super-resolution; density matrix

Introduction

Optical microscopy is at the heart of analysis in biology, used at scales ranging from systemic to sub-cellular. Important recent developments are far-field sub-diffraction-limited resolution imaging techniques that have opened up new vistas for quantifying sub-cellular features.

Notable examples of far-field sub-diffraction-limited resolution imaging are stimulated emission depletion (STED) microscopy,[1,2] photoactivated localization microscopy (PALM),[3] and stochastic optical reconstruction microscopy (STORM).[4,5] STORM and PALM require that the fluorescent emitters be sufficiently spaced so that by careful activation and deactivation single-photon detection and counting statistics can be used to fit centriod locations far more accurately than the diffraction-limited spot. STORM and PALM have long image acquisition times, so that cells must be fixed before imaging. Finally, the careful activation and deactivation process requires rather specialized fluorescent labels.[6]

STED microscopy[1] exploits the optical nonlinear process of saturation; the population of fluorophores is excited by a light field, and then selectively depleted by another light field that stimulates the fluorophores to emit. This suppresses the spontaneous fluorescence from the fluorophore population, effectively limiting it to locations where the stimulating light field is less than the saturation intensity of the label molecule. Using a stimulating light field with a node at the center limits the spontaneous fluorescence to emission from a sub-diffraction-limited volume at the beam center. Furthermore, the resolution increases with the square root of the intensity of the additional laser beam, allowing one to tune the resolution. Recent results show that STED can provide images with a lateral resolution of 6 nm in solids[7] or 33 nm in liquids.[8]

Label-free imaging techniques, such as coherent anti-Stokes Raman scattering (CARS) microscopy, have the benefit of not complicating observations through the introduction of fluorescent

* *Correspondence to: Klaus J. Boller, Laser Physics and Nonlinear Optics Group, MESA+ Research Institute for Nanotechnology, University of Twente, P. O. Box 217, Enschede 7500AE, The Netherlands. E-mail: k.j.boller@utwente.nl*

† *This article is part of the Journal of Raman Spectroscopy special issue entitled "Proceedings of the 9th European Conference on Nonlinear Optical Spectroscopy (ECONOS), Bremen, Germany, June 21–23, 2010" edited by Peter Radi (PSI, Villigen, Switzerland) and Arnulf Materny (JacobsUniversity, Bremen, Germany).*

a *Laser Physics and Nonlinear Optics Group, MESA+ Research Institute for Nanotechnology, University of Twente, Enschede 7500AE, The Netherlands*

b *Institut für Angewandte Physik, Westfälische Wilhelms-Universität, 48149 Münster, Germany*

c *Optical Sciences Group, MESA+ Research Institute for Nanotechnology, University of Twente, Enschede 7500AE, The Netherlands*

 Copyright © 2011 John Wiley & Sons, Ltd.

Journal of RAMAN SPECTROSCOPY

labels before imaging. By using characteristic vibrational modes to identify and track features, CARS microscopy can provide high-contrast video rate imaging. In addition, the laser fields are nonresonant, limiting photodamage.[9] It is of considerable interest to achieve sub-diffraction-limited CARS imaging, and several research groups are actively investigating linear and nonlinear techniques.[10,11] However, linear techniques cannot be used to increase the spatial frequency cutoff of an imaging system to obtain sub-diffraction-limited resolution, leaving only nonlinear optical processes.

In this paper, we present a density matrix model[12] of CARS emission. CARS emission in a four-level system (Fig. S1, Supporting information), where another light field couples a level, referred to as the control level, $|4\rangle$, to the ground-state $|1\rangle$, is considered. Two mechanisms that lead to sub-diffraction-limited CARS microscopy may have been identified. When the population in the control level can be rapidly transferred to the vibrational level ($|2\rangle$) via an incoherent process, then the buildup of the vibrational coherence is suppressed, which reduces the CARS emission.[13] When the lifetime of $|4\rangle$ and the dephasing of the $|1\rangle - |4\rangle$ transition is sufficiently long compared to the transition rate imposed by the additional laser, Rabi oscillations between $|1\rangle$ and $|4\rangle$ result, inducing a Rabi splitting of the CARS emission.[14] The Rabi splitting is intensity-dependent, which can be used to identify features within a diffraction-limited volume (reminiscent of the work performed by Gardner *et al*.[15]).

Theoretical Framework

The level scheme of the medium and the driving light fields used in our calculations are shown in Fig. S1. The four-level system contains a ground state ($|1\rangle$), a vibrational state ($|2\rangle$), an excited state ($|3\rangle$), and a control state ($|4\rangle$). Transitions between the ground and excited states, the vibrational and excited states, as well as the ground and control states, are dipole-allowed, while all other transitions are dipole-forbidden.

The pump, Stokes, and probe pulsed laser fields, with frequencies ω_p, ω_S, and ω_{pr}, illuminate the medium. Although these fields are far detuned from the $|1\rangle - |3\rangle$ and $|2\rangle - |3\rangle$ transition frequencies, the pump and Stokes lasers are in two-photon resonance with the $|1\rangle$ and $|2\rangle$ transition. This populates $|2\rangle$, creating a population difference between the states $|1\rangle$ and $|2\rangle$, which, in combination with the two-photon resonant light fields, builds up the vibrational coherence. The vibrational coherence induces optical sidebands on the probe light frequency, one of which is the CARS emission frequency ($\omega_c = \omega_p - \omega_S + \omega_{pr}$). Often, the laser fields ω_p and ω_{pr} are chosen to be degenerate in frequency; however, for clarity, we use two different laser fields for ω_p and ω_{pr}.

To understand how the additional laser (called the control laser ω_{ct}) influences CARS emission, we calculate the dynamics of the envelopes of the density matrix elements with the Liouville equation[16] $d\rho/dt = -i/\hbar[H, \rho] - (\Gamma_{ij}\rho_{ij})$. The Hamiltonian H (in dipole approximation) contains the pump, probe, and Stokes laser fields, plus the control laser, with frequency ω_{ct}, chosen to be resonant with the $|1\rangle - |4\rangle$ transition.

We study the following two cases: the incoherent population exchange rate between levels $|4\rangle$ and $|2\rangle$ is considered to be high (0.1 THz) (see Section on Saturable Suppression of CARS); and CARS emission for the case where $|4\rangle$ has a decoherence rate that is slow compared to the duration of the laser pulses (see Section on Rabi Modulation of CARS). The former results in a rapid equalization of population between $|4\rangle$ and $|2\rangle$. Although this appears to be a special case, the vibrational modes of complex organic molecules meet this requirement, because they often cross-relax on relatively short time scales.[17] In the latter case, the slow decoherence results in Rabi oscillations between $|1\rangle$ and $|4\rangle$. Although in our calculations $|4\rangle$ is treated as a vibrational state, any dipole-allowed state with the requisite decoherence rate may be used. A study of the literature reveals that appropriate vibrational states can be found.[18]

In our calculations, the incident light fields E_{ij} are taken as the sum of the pulse envelopes from the pump, Stokes, probe, and control light fields: $E_{ij} = \sum_n A_n \exp(i\Delta_{ij}t)$, where $n = \{p, S, pr, ct\}$. $A_n(t)$ is the Gaussian shaped pulse envelope, $\Delta_{ij} = \omega_n - \omega_{ij}$, with ω_{ij} being the transition frequency. We have assumed that there is no temporal delay between the light pulses of the pump, probe, and Stokes fields. In order to prepare the state of the medium, the control pulse arrives and terminates before the onset of the other pulses.

The off-diagonal density matrix elements $\rho_{13}(t)$ and $\rho_{23}(t)$ act as the source terms of radiation in the Maxwell equations.[12] We obtain the full temporal development of these elements by multiplying the envelopes $\rho_{ij}(t)$ with their respective transition frequencies. The Fourier transform of this provides the spectrum of the emitted radiation.

To investigate the coherent and incoherent saturation of CARS, we have chosen parameters that are typical, rather than specific, to a particular molecule. The $|1\rangle - |3\rangle$, $|1\rangle - |2\rangle$, and $|1\rangle - |4\rangle$ transition frequencies are taken to be 1000 THz ($\sim$300 nm, $\sim$33 000 cm^{-1}), 47 THz ($\sim$6.4 μm or $\sim$1550 cm^{-1}), and 97 THz ($\sim$3.1 μm or $\sim$3200 cm^{-1}), respectively. The pump and Stokes light fields are set to be two-photon-resonant with the $|1\rangle - |2\rangle$ transition, with the resulting pump and Stokes detunings of $\Delta_p = \Delta_S = 353$ THz, measured with respect to the $|1\rangle - |3\rangle$ and $|2\rangle - |3\rangle$ transitions, respectively. The detuning of the probe, Δ_{pr}, is set to 200 THz with respect to the $|1\rangle - |3\rangle$ transition. This corresponds to pump, Stokes, and probe wavelengths of 800, 923, and 600 nm. The remaining parameters are given in the next Section and the Section on Rabi Modulation of CARS.

Saturable Suppression of CARS

For the incoherent saturable suppression of CARS, the $|1\rangle - |2\rangle$ and $|1\rangle - |4\rangle$ transition frequencies are chosen to be close to each other to allow for a high nonradiative population transfer rate, which we take to be 0.1 THz. The total lifetime of $|3\rangle$ is taken to be short, in the order of picoseconds. The lifetimes of $|2\rangle$ and $|4\rangle$ are taken to be in the order of nanoseconds, while the coherence lifetimes between each other and $|1\rangle$ is of the order of picoseconds.[19–21] The laser pulse durations, τ, are 2 ps ($1/e^2$, full width half-maximum (FWHM)), except for the control pulse, which is 35 ps in duration and arrives 60 ps in advance of the pump, Stokes, and probe pulses. The simulations were performed numerically, using a fourth-order Runge–Kutta solver over a time range 100 ps in steps of 2.5 attoseconds.

As can be seen in Fig. 1(a), the control pulse populates $|4\rangle$ to a density that depends on the pulse energy of the control pulse. The high transition rate between $|2\rangle$ and $|4\rangle$ ensures that the population density of $|2\rangle$ closely follows that of $|4\rangle$. This process saturates for a critical pulse area[22] of about 100 radians for this particular case (maximum Rabi frequency multiplied by the pulse duration). The influence of this saturation process is shown in Fig. 1(b), where the pre-pulse has the effect of suppressing CARS

 Copyright © 2011 John Wiley & Sons, Ltd.

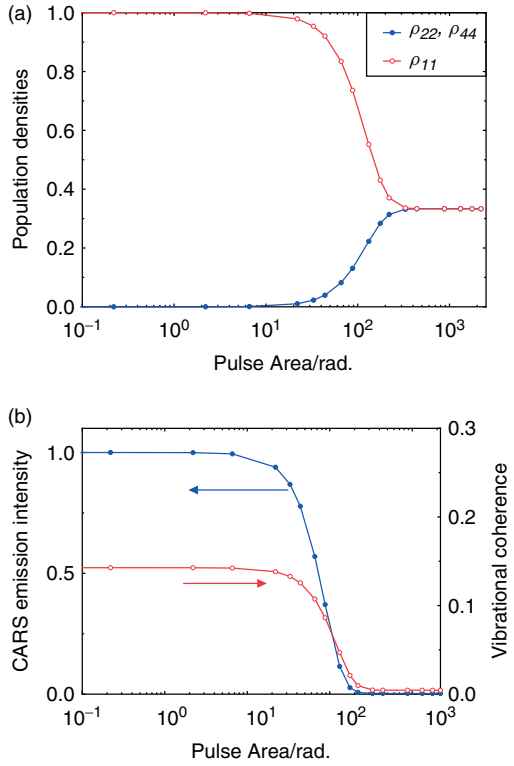

Figure 1. (a) Typical population densities as a function of control laser pulse area. A significant fraction of the ground state population is transferred to $|4\rangle$ and, via nonradiative transitions, to $|2\rangle$ once the control pulse area is large. (b) Vibrational coherence ρ_{12} (grey) and corresponding CARS emission intensity (black) as a function of control laser pulse area. The vibrational coherence is suppressed and CARS emission is saturated by the control laser pulse beyond a pulse area of ~100 radians.

emission. For our parameters, we observe that CARS emission can be suppressed to a maximum of 99.8% compared to the normal intensity of CARS emission.

From the saturation process, a saturation intensity can be defined as the control pulse intensity that frustrates CARS emission to one-half of its maximum value[22] This saturation intensity corresponds to a 25% reduction of the ground state population density. We note that vibrational population inversion and 50% ground state depletion of biologically relevant samples by direct excitation using a mid-IR laser has been observed by Ventalon *et al.*[23] The reported pulse duration, pulse energy, and the bandwidths of the vibrational states were used to estimate that the populations of their ground state and first vibrational state become equalized at intensities in the order of 70 GW/cm^2 during a 100 fs pulse. Although this is high, it is important to note that the *pulse area* of the control laser is more important than the intensity. Hence, we estimate that a control pulse with a longer pulse duration, such as the 35 ps duration used in our example, requires an intensity of just 200 MW/cm^2. This is well below the threshold for multiphoton ionization and excitation in the mid-infrared.

We estimate the resolution enhancement by considering an experimental setup wherein the control laser illuminates the sample with a donut mode, focused to a diffraction-limited spot. We define the node of the control laser beam to the area where the control laser's intensity is lower than the saturation intensity. CARS emission from within the node is unsuppressed, thus largely unaltered, while outside the node it is suppressed by up to 99.8%.

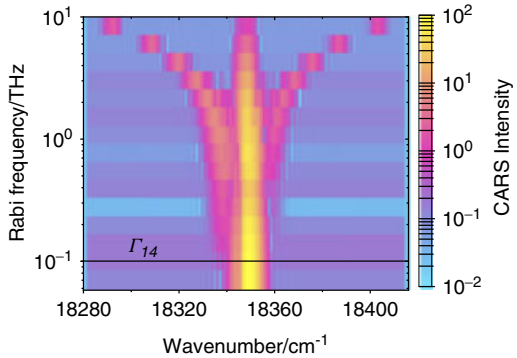

Figure 2. CARS emission spectra as a function of the control-laser-induced Rabi frequency oscillations. Note that the sidebands are notable only when the Rabi frequency is greater than the decoherence rate, Γ_{14}, as indicated by the black line. The position of the sidebands relative to the central peak is equal to Ω_R.

However, as the control laser intensity is increased, the node becomes smaller and the total CARS emission from within the node decreases, placing an upper limit on the resolution. The best resolution can then be considered to be defined by the radius of the node for which the signal contribution from within the node is greater than the signal contribution from outside the node. This allows us to derive an upper limit to the improved resolution of approximately $\lambda/(22\ \mathrm{NA})$, where NA is the numerical aperture of the imaging system and λ is the wavelength of the probe beam.

These calculations show that sub-diffraction-limited resolution images can be obtained by extending the standard CARS microscopy setup to include a mid-IR control laser beam with a donut-shaped transverse profile. This laser should be resonant with an appropriate vibrational transition and have an intensity above the saturation intensity of the vibrational transition. The node leaves the CARS process unaffected in a sub-diffraction-limited space around the center of the common focus, whereas CARS emission from that area outside the node is suppressed. The measured CARS signal can then be attributed to this sub-diffraction-limited region, where the intensity is less than the saturation intensity.

Rabi Modulation of CARS

Unlike in the previous section, longer lifetimes are chosen, with $R_{41} + R_{42}$ of state $|4\rangle$ are on the order of nanoseconds.[20] The decoherence rates between states are of the order of picoseconds.[19–21] All the laser pulse durations, τ, are set to 7 ps ($1/e^2$, FWHM) except for the control laser field, which is continuous during the interval of CARS emission. The numerical calculations extend over 30 ps in steps of 0.1 attoseconds.

To understand how the control laser modifies the CARS emission spectrum, the amplitude of the control field and, hence, the Rabi frequency (Ω_R) were varied in steps with the decoherence rate, Γ_{14}, held fixed at 0.1 THz. As shown in Fig. 2, the spectrum of the CARS emission is single-peaked when $\Omega_R < \Gamma_{14}$. However, once the Rabi frequency is larger than the decoherence rate, the spectrum of the CARS emission splits so that there are two symmetrical sidebands. These sidebands show a spacing from the CARS carrier frequency that coincides with Ω_R, given by the following equation[12]:

$$\Omega_R = \sqrt{\frac{E_c^2 \mu_{14}^2}{\hbar^2} + \Delta_{14}^2} \qquad (1)$$

Copyright © 2011 John Wiley & Sons, Ltd.

Journal of RAMAN SPECTROSCOPY

In this expression, $E_c = \sqrt{(2I_c/\epsilon_0)}$ is the control laser's electric field, and μ_{14} is the dipole moment at the $|1\rangle - |4\rangle$ transition. Examination of the ground state population as a function of time showed that the Rabi oscillations periodically deplete the ground state, which modulates the vibrational coherence. As a result, the amplitude of the CARS emission is modulated, creating two Rabi sidebands in the CARS emission spectrum. The splitting, which is large enough to overcome the decoherence, is several terahertz, which is large enough to be distinguishable in a real CARS experiment using standard spectrum analyzers.

This condition is further illustrated in Fig. S2, Supporting information. It can be seen that the sidebands are noticeable only if the Rabi frequency exceeds the decoherence rate. In these simulations, the Rabi frequency is held fixed, while the decoherence rate varies from 0.02 to 10 THz. Up to the decoherence rates, corresponding to sub-picosecond decoherence times, the 4 THz modulation is still detectable in Fig. S2. Since liquids have short coherence times – typically on the order of 5 ps[18] – obtaining high Rabi frequencies is important to observe the presence of the sidebands.

The frequency of the sidebands depends on the intensity of the control laser (Eqn (1)), which can be used to obtain sub-diffraction-limited resolution. The radial distance between the emitter and the center of the control beam can be calculated by measuring the exact frequency of the sidebands, which we refer to as Rabi labeling of the emitter position. The spatial dependence of the Rabi frequency is well known,[24] however, it is usually considered to cause undesired broadening and should, therefore, be eliminated.[25]

The absolute position of an emitter location can be calculated by trilateration in either two or three dimensions. Consider, as a two-dimensional example, an emitter located at the Cartesian coordinates x_1 and y_1. The frequency of the CARS sidebands depends on the local intensity of the control laser, and cannot be used to determine either of these coordinates directly. Instead, the sideband frequency corresponds to the distance between the center of the control beam and the emitter, $r_1 = \sqrt{x_1^2 + y_1^2}$. Scanning the control laser by a known distance dx along the x-axis results in the radial location of the emitter changing to $x_1 - \mathrm{d}x, y_1$. The sideband frequency change reveals a new control beam center-to-emitter distance, $r_2 = \sqrt{(x_1 - \mathrm{d}x)^2 + y_1^2}$. Solving these two expressions for x_1 yields $x_1 = (r_1^2 - r_2^2 - \mathrm{d}x^2)/(2\mathrm{d}x)$. A similar procedure provides y_1. Clearly, the resolution of such an imaging process will depend on how well resolved the sidebands are. In the following, we show that sub-diffraction-limited resolution is possible.

Consider the pump, Stokes, probe, and control laser all centered on the same location and focused to their respective diffraction-limited Gaussian-shaped intensity profiles. The distribution of emitters then generates a distribution of Rabi sidebands on the CARS signal. The range of the Rabi sidebands is given by $\Omega_{max} = |\mu_{14}E_0/\hbar|$ in the center to $\Omega_{min} = 1/e|\mu_{14}E_0/\hbar|$ at a radial distance w_0, where E_0 is the peak of the control laser field envelope and w_0 is the a $1/e$ spot size of the control laser. The radial resolution then depends on how accurately the content of the Rabi sidebands are determined. Given a Rabi frequency Ω corresponding to a radial distance from the center of the focus r and an optical frequency measurement accuracy dΩ, the corresponding radial resolution is dr. It can be shown that

$$\mathrm{d}r = \frac{w_0^2}{2r + \mathrm{d}r} \ln\left(\frac{\Omega}{\Omega - \mathrm{d}\Omega}\right) \qquad (2)$$

The transcendental Eqn (2) indicates that dr can be made smaller than the diffraction-limited beam waist w_0 of the probe beam by increasing the Ω. Furthermore, emitters located away from the center of the control beam are resolved better than those close to the center due to the presence of 2r in the denominator. Equation 2 reveals that, for a given control laser intensity, the resolution reaches its maximum value where the steepest intensity slope of the control laser beam is. Hence, by using a Gaussian-shaped control beam, the highest resolution is expected to be found off the center. We illustrate this for a range of Rabi wavenumbers in Fig. S3, Supporting information, where we have plotted the Rabi-labeling resolution as a function of both Rabi wavenumber and radial location. In this case, we use $\mathrm{d}\Omega = 3\ \mathrm{cm}^{-1}$, which is a typical value for the line width of a vibrational resonance in liquid. This figure shows that considerable improvement over diffraction-limited CARS microscopy is possible.

For a specific implementation of a microscope with a numerical aperture of 1.2 and the laser wavelengths that were used in our calculations, the diffraction-limited resolution is 171 nm. If the control laser with a wavelength of $\lambda = 3.3\ \mu\mathrm{m}$ and focused to a diffraction-limited spot induces $100\ \mathrm{cm}^{-1}$ Rabi oscillations, then at a radial distance of 1.2 µm the resolution is 65 nm. From the data presented in Ref. [18], we estimate that $100\ \mathrm{cm}^{-1}$ Rabi oscillations can be generated with a control laser intensity of about $500\ \mathrm{MW/cm}^2$. This intensity is comparable to the intensities used in standard CARS experiments, and is sufficiently low to avoid multiphoton excitation.[23]

Conclusions

We have used a density matrix model of a four-level system to demonstrate two routes to obtaining sub-diffraction-limited resolution in CARS microscopy. In the first approach, a STED-like process was described. In this approach, an intense control laser beam was shown to be able to suppress CARS emission in a saturable way. To achieve this, it is necessary for the control laser to pre-populate a vibrational state that is nonradiatively coupled to the vibrational state probed by the CARS process. Using typical parameters for molecular transitions probed by CARS microscopy, we showed that up to 99.8% saturation could be obtained. We estimate that the upper limit on sub-diffraction-limited resolution is $\sim\lambda/(22\ \mathrm{NA})$, where λ is the wavelength of the probe beam. The required pulse area for saturation corresponds to intensities that span a range from $200\ \mathrm{MW/cm}^2$ through to $100\ \mathrm{GW/cm}^2$, which seems tolerable since the molecules remain in their electronic ground state.

For control transitions with longer coherence times, we have shown that resonantly driving the excitation of the control state results in intensity and, thus, spatially dependent sidebands in the CARS emission spectrum. Accurately measuring the resulting Rabi splitting in the CARS spectrum allows objects to be resolved to a resolution below the diffraction limit. We estimate from typical experimental parameters that a resolution in the order of 65 nm may be achievable. We also note that our calculations show that any other emission process involving the ground-state, such as coherent Stokes Raman scattering, also generates Rabi sidebands, provided the decoherence rate is slower than the Rabi frequency. Hence, the Rabi labeling may be applicable to other microscopy techniques as well.

Supporting information

Supporting information may be found in the online version of this article.

 Copyright © 2011 John Wiley & Sons, Ltd.

References

[1] S. W. Hell, J. Wichmann, *Opt. Lett.* **1994**, *19*, 780.
[2] T. A. Klar, S. Jakobs, M. Dyba, A. Egner, S. W. Hell, *Proc. Natl. Acad. Sci. USA* **2000**, *97*, 8206.
[3] E. Betzig, G. H. Patterson, R. Sougrat, O. W. Lindwasser, S. Olenych, J. S. Bonifacino, M. W. Davidson, J. Lippincott-Schwartz, H. F. Hess, *Science* **2006**, *313*, 1642.
[4] B. Huang, S. A. Jones, B. Brandenburg, X. Zhuang, *Nat. Methods* **2008**, *5*, 1047.
[5] M. J. Rust, M. Bates, X. Zhuang, *Nat. Methods* **2006**, *3*, 793.
[6] R. Zenobi, *Anal.Bioanal. Chem.* **2008**, *390*, 215.
[7] E. Rittweger, K. Han, S. Irvine, C. Eggeling, S. Hell, *Nat. Photon.* **2009**, *3*, 144.
[8] M. Dyba, S. W. Hell, *Phys. Rev. Lett.* **2002**, *88*, 163901.
[9] Y. Fu, H. Wang, R. Shi, J. X. Cheng, *Opt. Express* **2006**, *14*, 3942.
[10] A. Nikolaenko, V. Krishnamachari, E. Potma, *Phys. Rev. A* **2009**, *79*, 7.
[11] V. Raghunathan, E. Potma, *J. Opt. Soc. Am. A* **2010**, *27*, 2365.
[12] P. W. Milonni, J. H. Eberly, *Laser Physics*, Wiley: Ney York, **2010**.
[13] W. P. Beeker, P. Groß, C. J. Lee, C. Cleff, H. L. Offerhaus, C. Fallnich, J. Herek, K. Boller, *Opt. Express* **2009**, *17*, 22632.
[14] W. P. Beeker, C. Lee, K. Boller, P. Groß, C. Cleff, C. Fallnich, H. L. Offerhaus, J. Herek, *Phys. Rev. A* **2010**, *81*, 012507.
[15] J. R. Gardner, M. L. Marable, G. R. Welch, J. E. Thomas, *Phys. Rev. Lett.* **1994**, *70*, 3404.
[16] Y. R. Shen, *The Principles of Nonlinear Optics* (Wiley Classics Library), Wiley-Interscience: New York, **2002**.
[17] H. Okamoto, K. Yoshihara, *Chem. Phys. Lett.* **1991**, *177*, 568.
[18] T. Witte, J. S. Yeston, M. Motzkus, E. J. Heilweil, K. L. Kompa, *Chem. Phys. Lett.* **2004**, *392*, 156.
[19] J. B. Asbury, T. Steinel, C. Stromberg, K. J. Gaffney, I. R. Piletic, A. Goun, M. D. Fayer, *Phys. Rev. Lett.* **2003**, *91*, 2374021.
[20] R. de Vivie-Riedle, U. Troppmann, *Chem. Rev.* **2007**, *107*, 5082.
[21] A. J. Wurzer, T. Wilhelm, J. Piel, E. Riedle, *Chem. Phys. Lett.* **1999**, *299*, 296.
[22] B. Hein, K. I. Willig, S. W. Hell, *Proc. Natl. Acad. Sci. USA* **2008**, *105*, 14271.
[23] C. Ventalon, J. M. Fraser, M. H. Vos, A. Alexandrou, J. L. Martin, M. Joffre, *Proc. Natl. Acad. Sci. USA* **2004**, *101*, 13216.
[24] P. Schouwink, H. Berlepsch, L. Dahne, R. F. Mahrt, *Chem. Phys.* **2002**, *285*, 113.
[25] V. A. Sautenkov, C. Y. Ye, Y. V. Rostovtsev, G. R. Welch, M. O. Scully, *Phys. Rev. A* **2004**, *70*, 033406.

Copyright © 2011 John Wiley & Sons, Ltd.